Quasi-Dynamic Homogenization of Geometrically Simple Dielectric Composites

Jiaran Qi, Henrik Kettunen, Henrik Wallén, and Ari Sihvola

Aalto University School of Science and Technology
P.O. Box 13000, FI–00076 AALTO, Finland
qi.jiaran@tkk.fi

Abstract ─ The frequency dependence of the effective permittivities of simple dielectric composites is evaluated by different quasi-dynamic homogenization methods. Three retrieval approaches based on the scattering parameters are proposed for dielectric materials. A compensation method for the conventional Nicolson-Ross-Weir (NRW) retrieval is applied to eliminate the Fabry-Pérot (FP) resonances and their distortions of the retrieval results. All these quasi-dynamic homogenization methods are then evaluated by comparing the corresponding retrieval results against one another. Finally, by comparing these retrieval results with the static Lord Rayleigh prediction, the limitation of the quasi-static approximation for such composites is considered.

Index Terms ─ Dispersion diagram, homogenization, Rayleigh mixing rule, S-parameter retrieval.

I. INTRODUCTION

Homogenization is a method whereby the complicated and spatially varying microscopic fields existing in a heterogeneous medium, when it is excited by an electromagnetic (EM) wave with sufficiently large wavelength, are replaced by smoothly varying (or macroscopic) fields. These fields can be used for characterizing the behavior of the medium with effective parameters [1, 2], the permittivity ε and the permeability μ. Indeed, depending on the symmetry, the arrangement and the intrinsic EM properties of the constituents of the composites, the effective bulk medium may exhibit anisotropic, bianisotropic, or chiral characteristics [3]. We, however, confine our focus to mixtures composed of linear, lossless, and passive dielectric materials, which in turn allows us to compress all EM properties approximately into the effective permittivity ε_{eff}.

In electrostatics, the permittivity of the effective bulk medium ε_{eff} can be successfully predicted by various classical mixing formulas. These mixing rules in general determine ε_{eff} in terms of the permittivity of the individual phases and their volume fractions for specific inclusion shapes. The Lord Rayleigh formula is taken due to its sufficient accuracy as the static prediction for the ε_{eff} of the composites of our interest in this paper. For spherical inclusions (ε_{i}) with volume fraction p dispersed in the host medium (ε_{e}), the Rayleigh effective permittivity ε_{Ray} reads [4],

$$\varepsilon_{\text{Ray}} = \varepsilon_{\text{e}} + \frac{3p\varepsilon_{\text{e}}}{\dfrac{\varepsilon_{\text{i}} + 2\varepsilon_{\text{e}}}{\varepsilon_{\text{i}} - \varepsilon_{\text{e}}} - p - \dfrac{1.305 \cdot p^{10/3}\left(\varepsilon_{\text{i}} - \varepsilon_{\text{e}}\right)}{\varepsilon_{\text{i}} + 4\varepsilon_{\text{e}}/3}} . \quad (1)$$

When the scale of the local inhomogeneity is, however, no longer very small compared with the wavelength of the applied fields, the validity of the quasi-static description of heterogeneous media with effective medium parameters becomes a critical issue.

With the recent emergence of metamaterials, many researchers [5, 6] had extended such a homogenization procedure into this sensitive region, where the dimension of unit cell is usually an appreciable fraction of the wavelength [7], to characterize their EM properties with the effective medium parameters ε and μ. On the contrary, in [8] the authors found that the conventional effective material parameters are meaningless for an optical fishnet metamaterial due to the mesoscopic nature and the related spatial

dispersion. Instead of questioning its validity, we discuss in this paper how far upwards in frequency range we can approximately apply the static permittivity. We explore this problem by considering the quasi-dynamic homogenization of two kinds of simple composites — a transversally infinite slab and a simple cubic lattice, and constrain the homogenization of the slab to only one of the principal axes to eliminate the spatial dispersion influences. It is furthermore assumed that the constituents of the composites are dielectric materials and no artificial magnetism is generated by the homogenization. In order to determine the limit of the quasi-static approximation, we present four different S-parameter-based methods and the *ka–βa* dispersion diagram method [9] to retrieve the frequency dependence of the effective permittivity of two composites, and then compare them with the corresponding static Lord Rayleigh prediction to decide up to what extent it still holds the predictive power. It is moreover demonstrated that below such limits the spatial dispersion can be neglected for the simple cubic lattice.

II. GEOMETRY SETUP

Composites are analyzed in this paper using two models. The first one is a slab of thickness *d* which is infinite in the transverse direction (*x* and *y*) and formed from 9 cubic unit cells in *z* direction, while the other one is an infinite simple cubic lattice. Both composites are composed of the same unit cells. The unit cell is constructed by a dielectric spherical inclusion with relative permittivity ε_i centered in a dielectric cube ($\varepsilon_e = 1$) with edge length *a*, and the inclusion volume fraction is *p*. In this paper, we use the 3D EM simulator CST Microwave Studio (CST MWS) [10] to compute the required data for the ε_{eff} retrievals of different mixtures.

A. The slab

We consider the situation when a plane wave with *y*-polarized electric field is normally incident on the transversally infinite slab. Such a scenario can be realized by a finite structure with proper boundary conditions in CST MWS, due to the symmetry of the field distribution. As shown in Fig. 1, a slab of thickness *d* is made of 9 unit cells in a row, and an additional free space is added to prevent higher modes from propagating. PEC boundary conditions are assigned to the slab's upper and lower surfaces in *y* direction, while in *x* directions PMC boundaries are given. The whole geometry is then excited by two waveguide ports, which as well compute the S-parameters for retrievals. Only the electric response in *y* direction is of interest due to the *y*-directionally polarized electric field. Since the whole structure is symmetric with respect to the *xz* and *yz* planes, the computational complexity can be reduced by defining them respectively as electric and magnetic symmetry planes. Therefore, merely one quarter of the structure needs to be computed.

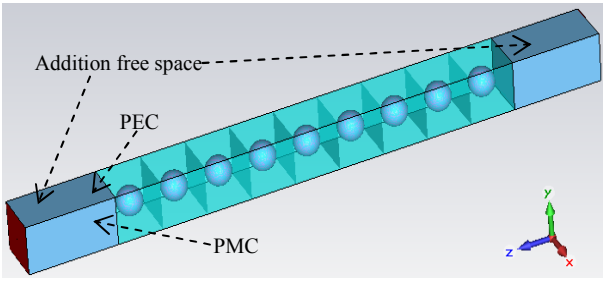

Fig. 1. 3D simulation configuration for the nine layer transversally infinite slab in CST MWS.

B. The simple cubic lattice

The simple cubic lattice can be constructed in CST MWS readily by assigning periodic boundary conditions to all six surfaces of the cubic unit cell. The *ka–βa* dispersion diagrams of the TEM modes for three different propagation directions, along the cube edge, surface diagonal and volume diagonal, are then generated respectively for retrievals.

III. RETRIEVAL METHODS

Many sophisticated techniques have been employed for the practical measurements to estimate the dielectric properties of materials [11]. But the full wave simulator, which eliminates many realistic uncertainties, enables us to retrieve the permittivities of the proposed composites with more straightforward methods. In this section, different retrieval methods will be introduced targeted on different composites. For the slab, four S-parameter-based methods are applied, while the *ka–βa* dispersion diagram approach is presented for the infinite lattice.

A. The slab case — S-parameter-based methods

1. The conventional NRW method

The classical approach of retrieving the effective ε and μ from S-parameters was originally studied by Nicolson, Ross, and Weir [12, 13]. Smith and coauthors improved and extended this method to determine the effective medium parameters of metamaterials [14]. Later, Chen and coauthors presented a more robust method aiming at metamaterials as well [15]. For a plane wave normally incident on a homogeneous slab with thickness d, the simulated S-parameters are related to n and z by [15]:

$$z = \pm\sqrt{\frac{\left(1+\mathrm{S}_{11}\right)^2-\mathrm{S}_{21}^2}{\left(1-\mathrm{S}_{11}\right)^2-\mathrm{S}_{21}^2}}. \tag{2}$$

$$Q = e^{-jnkd} = \frac{\mathrm{S}_{21}}{1-\mathrm{S}_{11}\dfrac{z-1}{z+1}}. \tag{3}$$

$$n = \frac{1}{kd}\left\{\left[-\mathrm{Im}\left[\ln\left(Q\right)\right]+2m\pi\right]+j\cdot\mathrm{Re}\left[\ln\left(Q\right)\right]\right\}, \tag{4}$$

where k denotes the free space wave number. The sign ambiguity in Eq. (2) can be cleared by the requirement $\mathrm{Re}(z) \geq 0$. Once z is determined, the imaginary part of the refractive index n will be solved by Eq. (3) and (4). The branch index m (integer value) of the logarithm function is then decided by the non-magnetic presumption. The effective permittivity and permeability can, hence, be directly calculated from the refractive index n and the impedance z by $\varepsilon_{\mathrm{eff}} = n/z$, $\mu_{\mathrm{eff}} = nz$.

2. Retrieval from either S_{11} *or* S_{21}

It is important to notice that for nonmagnetic materials with the assumption $\mu_{\mathrm{eff}} = 1$, when a plane wave is normally incident on a homogenous slab with thickness d, the gap between S-parameters and medium parameters $\varepsilon_{\mathrm{eff}}$ can also be bridged by the following equations,

$$\mathrm{S}_{11} = \frac{R\left(1-e^{-j2\sqrt{\varepsilon_{\mathrm{eff}}}kd}\right)}{1-R^2e^{-j2\sqrt{\varepsilon_{\mathrm{eff}}}kd}}. \tag{5}$$

$$\mathrm{S}_{21} = \frac{\left(1-R^2\right)e^{-j\sqrt{\varepsilon_{\mathrm{eff}}}kd}}{1-R^2e^{-j2\sqrt{\varepsilon_{\mathrm{eff}}}kd}}, \tag{6}$$

where $R = (z-1)/(z+1) = (1-\varepsilon_{\mathrm{eff}}^{1/2})/(1+\varepsilon_{\mathrm{eff}}^{1/2})$. Both Eq. (5) and (6) then become functions of only one variable $\varepsilon_{\mathrm{eff}}$, meaning either S_{11} or S_{21} contains sufficient information for the retrieval. In other words, this fact enables us to retrieve the effective permittivity from either one of S-parameters by solving the complex roots of Eq. (5) or (6).

3. Effective wavelength retrieval (EWR)

For a lossless slab, the FP resonances will occur when the thickness of the slab d is equivalent to an integer t multiple of one half of the effective wavelength of the field inside the slab. In this occasion, there is no reflection, i.e., $\mathrm{S}_{11} = 0$. From either the above condition or Eq. (5), we have $\exp(-j2nkd) = 1$, which gives the following equation,

$$\varepsilon_{\mathrm{eff}} = \left(\frac{t\lambda_t}{2d}\right)^2, \qquad t = 1,2,3... \tag{7}$$

where λ_t is the free space wavelength at the FP resonance of order t. Although this method is only valid for the retrieval at frequency points corresponding to the FP resonances, it provides a good comparison and validation for the results by other retrieval approaches.

In particular, the FP resonance and its influence on the retrieved results are usually neglected in the previous literature, partially due to the narrow retrieval frequency band. Another major factor is that the test samples are usually lossy materials, such as various kinds of metamaterials.

B. The lattice case ─ *ka–βa* method

The frequency dependence of the $\varepsilon_{\mathrm{eff}}$ of the infinite simple cubic lattice can be addressed as long as the *ka–βa* dispersion diagram is obtained, given that the effective wave number β is related to k by $\beta = k\,\varepsilon_{\mathrm{eff}}^{1/2}$.

For an infinite lattice composed of nonmagnetic materials, the following eigenfunction can be derived from Maxwell equations [16],

$$\nabla\times\left(\frac{1}{\varepsilon(\boldsymbol{r})}\nabla\times\boldsymbol{H}(\boldsymbol{r})\right) = \left(\frac{\omega}{c}\right)^2\boldsymbol{H}(\boldsymbol{r}), \tag{8}$$

where $\boldsymbol{H}(\boldsymbol{r})$ denotes the magnetic field pattern of the harmonic mode, c is the free space light speed and ω represents the eigenfrequency. Only the TEM mode $\boldsymbol{H}(\boldsymbol{r}) = \boldsymbol{H}_0\,e^{-j\beta a}$ needs to be considered here. Then according to Eq. (8), under a certain propagation direction, the eigenfrequencies ω (or k) can be calculated by giving different phase shifts βa. The desired *ka–βa* dispersion diagram can thus be generated. In CST MWS, a certain propagation direction can be specified by

systematically varying the three phase shifts $\beta_x a$, $\beta_y a$, and $\beta_z a$ between the periodic boundary pairs in the x, y, and z directions. Three different propagation directions are considered in this paper for the simple cubic lattice — along the edge, the surface diagonal, and the volume diagonal of the cubic unit cell. The computed field pattern is then utilized to identify the direction of the retrieved ε_{eff}.

IV. RESULTS AND DISCUSSION

For the quasi-dynamic homogenization, an important parameter is the number of unit cells in one effective wavelength λ_{eff} at a certain frequency. We define the effective wavelength by reducing the free-space wavelength according to the static Rayleigh prediction, $\lambda_{\text{eff}} = \lambda/(\varepsilon_{\text{Ray}})^{1/2}$. But since the frequency dependence of ε_{eff} is also of our interest, we normalize the frequency to f_{20}, which denotes the frequency when the reduced wavelength is 20 times the length of the unit cell, $\lambda_{\text{eff}} = 20a$.

A. Compensation method

For the composite with $p = 0.1$, $\varepsilon_i = 10$, and $\varepsilon_e = 1$ shown in Fig. 1, the comparison of the retrieved effective permittivities by four S-parameter-based methods is visualized in Fig. 2. According to Eq. (1), the Rayleigh εeff for such a mixture is roughly 1.2434 (green dotted), and at low frequency all the results are in good agreement with this value. As the frequency increases, the effective permittivities gradually deviate from the static prediction and grow as expected. However, for the NRW (black solid), the FP resonances appear at 2.9851, 5.9617, 8.921, 11.851, and 14.738 GHz, and there is clearly a systematic leap following each FP resonance. For the S_{11} method (blue dot-dashed), the retrieved permittivity presents a small variation around the more stable results by the S_{21} approach (red dashed). As for the EWR (black dots), the results not only coincide as expected with those by S_{11} since the EWR is actually a special case of the S_{11} method, but follow closely those by the S_{21} method. The EWR therefore provides a good confirmation of the validity of the S_{21} method.

As shown in Fig. 2, the presence of the FP resonance prevents us from utilizing the results by the conventional NRW technique. In order to compensate its influence, the μ_{eff} by the NRW is also shown in Fig. 3. It can be seen that although we use the condition that μ_{eff} is closest to unity to settle the branch index m, the retrieved μ_{eff} leaps away from 1 after each FP resonance. A further investigation into the calculated n and z indicates

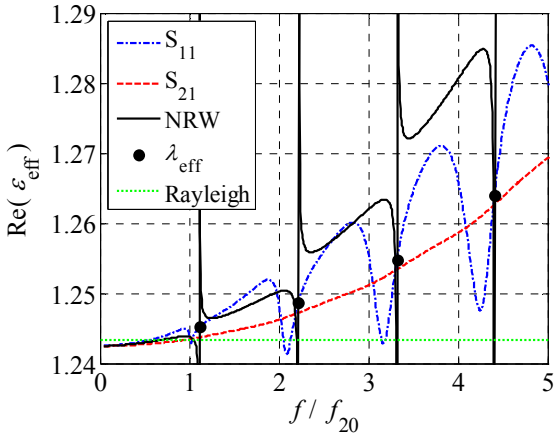

Fig. 2. The retrieved permittivities by four different S-parameter-based retrieval methods.

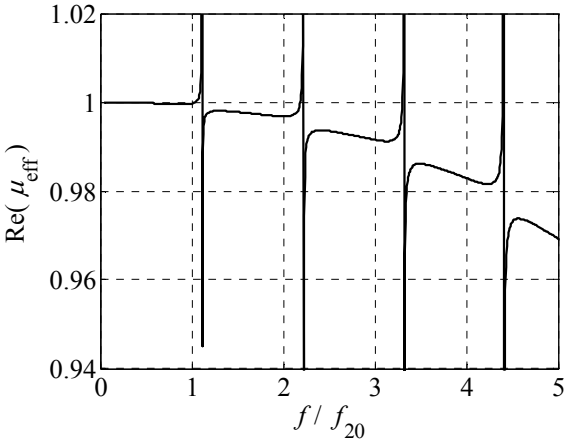

Fig. 3. The retrieved μ_{eff} by the conventional NRW method.

that the ill-retrieved z causes the abnormal leaps of the ε_{eff} and μ_{eff}, while the n displays reasonable frequency dependence. The effective permittivity can hence be calculated by $\varepsilon_{\text{eff}} = n^2$ instead of $\varepsilon_{\text{eff}} = n/z$, provided the nonmagnetic assumption $\mu_{\text{eff}} = 1$.

Figure 4 clearly illustrates that the compensated result has an excellent agreement with that by the S_{21} method. It should be noticed that since the electrical size of the dielectric inclusion (whose permittivity is reasonably low) is so small that the magnetic response can be

neglected, and since no other assumptions are applied, the compensation method does make physical and numerical sense. In addition, the compensated ε_{eff} is not exactly the same as that by the S_{21} method, suggesting that these two methods are independent of each other.

In particular, the unstable retrieval by the S_{11} method in Fig. 2 inspires us to study the imaginary parts of the ε_{eff}, respectively, by the S_{11} and S_{21} methods. Figure 5 illustrates that the S_{21} method is superior to the S_{11} method in that it manages to present clearly smaller values for the imaginary part of the ε_{eff} for this lossless mixture. This point shows that the S_{11} method is not suitable for such small reflection cases.

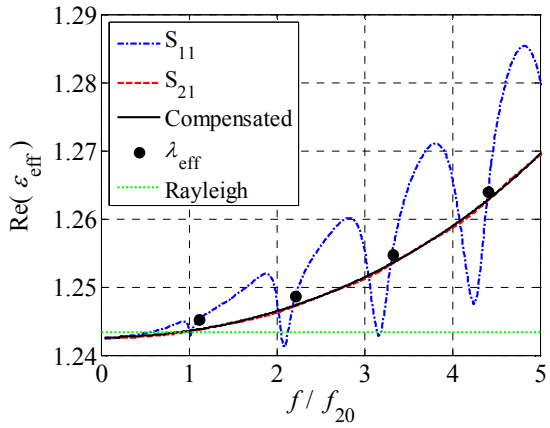

Fig. 4. The compensated result to the NRW method compared with those by the other three S-parameter-based approaches for the composites with $p = 0.1$, $\varepsilon_i = 10$, and $\varepsilon_e = 1$.

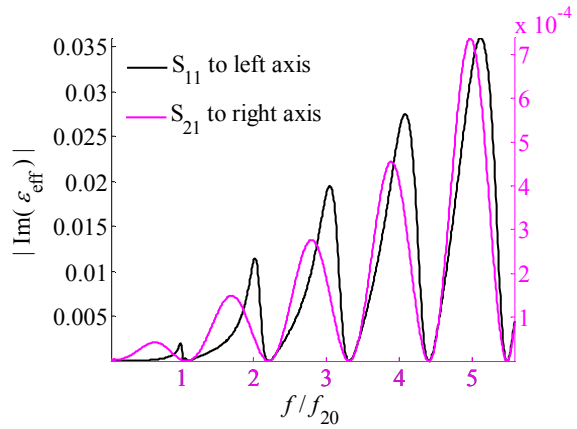

Fig. 5. Comparison between the imaginary part of the retrieved ε_{eff} by only S_{11} and that by only S_{21}.

B. *ka–βa* retrieval and spatial dispersion

Figure 6 visualizes the retrieved ε_{eff} for different wave propagation directions, and its legend provides not only the direction of propagation but also that of the field polarization. The 'SD–VD' (short for surface diagonal–volume diagonal), for instance, denotes the case when a plane wave travels along the surface diagonal of the cubic unit cell with a volume-diagonal-polarized electric field. As can be seen, the retrieved permittivities converge to the static Rayleigh prediction when the frequency decreases. For small values of f/f_{20}, the composite looks very isotropic, and the spatial dispersion becomes more apparent as the value of f/f_{20} increases over 2, i.e., a/λ_{eff} is larger than 1/10. Another interesting observation is that in this 3D scenario, waves propagating in different directions with the electric field in the same direction will result in the same dispersion curve. As shown in Fig.6, the 'Edge–Edge' curve agrees well with the 'SD–Edge' curve. Moreover, the dispersion curve when the electric field is polarised along the edge deviates most from the dotted curve predicted by the Rayleigh mixing rule, while the volume-directed electrical field leads to least deviation. The dispersion curve resulting from a surface-diagonal-directed electrical field lies between these two utmost cases.

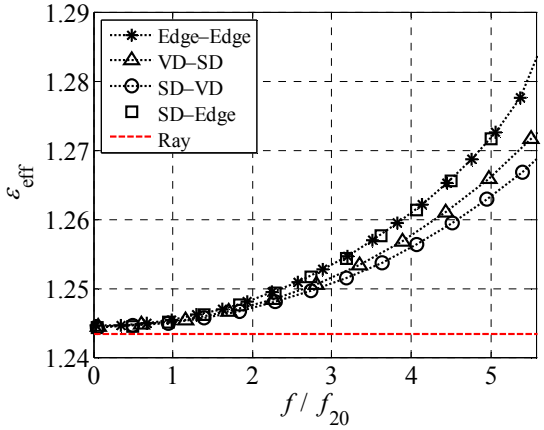

Fig. 6. The retrieval results for different directions of propagation when $p = 0.1$ and $\varepsilon_i = 10$. Note that the relative difference $|\varepsilon_{\text{Edge–Edge}} - \varepsilon_{\text{SD–VD}}| / \varepsilon_{\text{Ray}}$ is less than 1% up to 5 in terms of f/f_{20} (SD and VD stand for surface and volume diagonal).

C. Frequency dependence of ε_{eff} and quasi-static approximation limit

1. Frequency dependence of ε_{eff}

The one-principal-axis homogenization of the 9-layer slab (y direction) and the infinite simple cubic lattice (along the edge) are analyzed and shown in Fig. 7. The result shows that the permittivities of these two composites are in good agreement with one another, which further confirms the validity of all the presented ε_{eff} retrieval methods. In order for further validation, the ε_{eff} of these composites with the similar geometry but larger inclusions (p = 0.3) are considered. As shown in Fig. 8, the ε_{eff} of the slab along y direction and that of the lattice along the cube edge have a good match. Moreover, stronger spatial dispersion is observed, and the relative difference $|\varepsilon_{\text{Edge–Edge}} - \varepsilon_{\text{SD–VD}}| / \varepsilon_{\text{Ray}}$ is less than 1% up to 3.24 in terms of f/f_{20}.

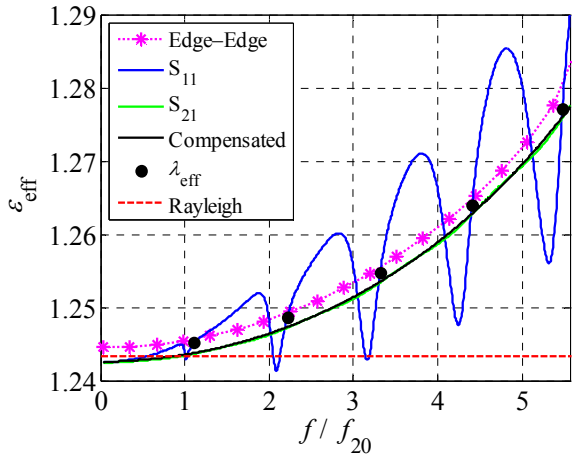

Fig. 7. The comparison among all the retrieved permittivities by different methods for p = 0.1 and ε_i = 10.

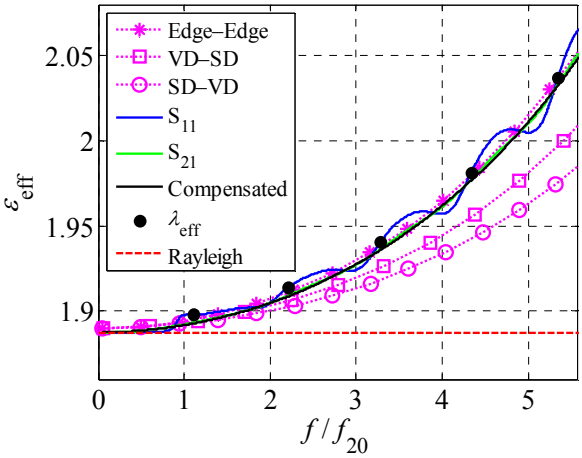

Fig. 8. The comparison among all the retrieved ε_{eff} by different methods for p = 0.3 and ε_i = 10.

It is also noted from Fig. 8 that the S_{11} method still seems unstable but the variation is much smaller than in Fig. 7 due to the increase of the targeted effective permittivity. For smaller p and moderate ε_i = 10, S_{11} is very small in amplitude and close to zero. When p increases, S_{11} becomes larger and thus less sensitive to the errors. So the tolerance of the S_{11} method could be improved as sufficiently large S_{11} is encountered, for instance, when the composites with a larger p or higher permittivity contrast are considered.

2. Quasi-static approximation limit

These results provide us possibilities to address the question regarding the limitations of the quasi-static homogenization principles for these dielectric composites with relatively small permittivity contrasts and volume fractions.

It is true that the homogenization with the effective constitutive parameters is in essence an approximation process, and may become less meaningful in the rigorous sense when the geometry details of the composites are not sufficiently small compared with the free-space or effective wavelength inside [8, 17]. However, it will be still interesting to quantitatively explore the limitation of the quasi-static approximation in a quasi-dynamic range by defining some criterion. In this paper, the relative difference between the retrieved ε_{eff} and the static Lord Rayleigh prediction ε_{Ray} is chosen as a proper target to be investigated, i.e., $|\varepsilon_{\text{eff}} - \varepsilon_{\text{Ray}}| / \varepsilon_{\text{Ray}}$.

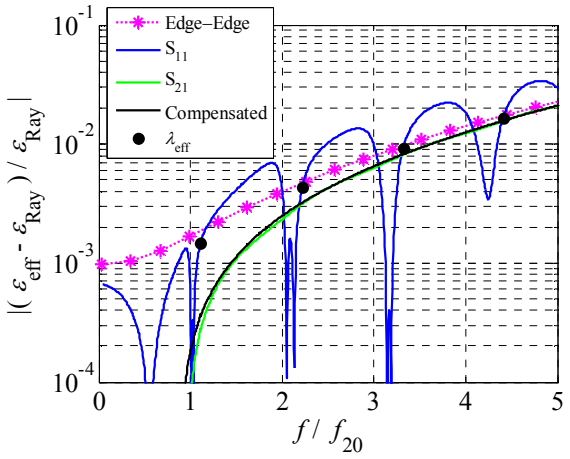

Fig. 9. The relative difference between all the retrieved permittivities and the static Rayleigh prediction for p = 0.1 and ε_i = 10.

Figures 9 and 10 illustrate the relative differences between the retrieved ε_{eff} and the static prediction ε_{Ray} for different p. Let us regard 1% relative difference as a satisfactory tolerance, and define the limit frequency meeting this criterion as f_{L}. Thus, the quasi-static approximation limit is denoted as f_{L}/f_{20}. Then for composites of our interest with different p, the one-principal-axis quasi-static approximation can be considered to be valid up to 3.5 and 2.1 in terms of f/f_{20}, correspondingly $a/\lambda_{\text{eff}} \approx$ 1/5.7 and 1/9.5. Within these limits, the relative difference between the ε_{eff} along the edge and the volume diagonal, i.e., $|\varepsilon_{\text{Edge–Edge}} - \varepsilon_{\text{SD–VD}}| \,/\, \varepsilon_{\text{Ray}}$, is also less than the 1% satisfactory tolerance for the cubic lattice. As a result, the spatial dispersion can be neglected below these quasi-static limits.

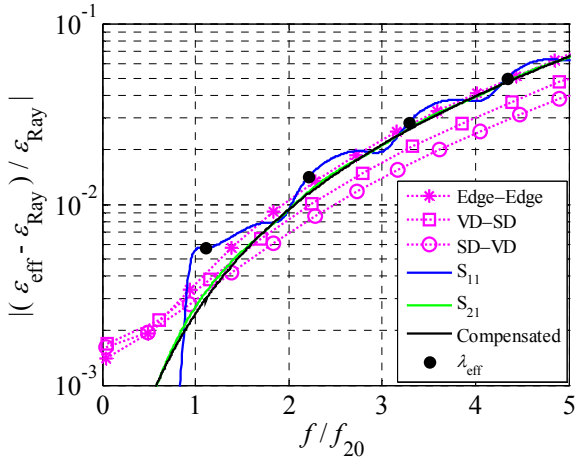

Fig. 10. The relative difference between all the retrieved permittivities and the static Rayleigh prediction for $p = 0.3$ and $\varepsilon_{\text{i}} = 10$.

To grasp the dependence of this limit on the inclusion properties, more composites, similar to that shown in Fig. 1 but with different ε_{i} and p, are considered and the computed limits f_{L}/f_{20} are shown in Table 1. It is shown that this limit decreases with the increase of either the permittivity contrast or the inclusion volume fraction. That is, for increasing frequency, the quasi-static approximation will lose its predictive power more quickly for the composite whose inclusions have stronger interactions.

3. Quasi-static limit for one-dimensional lattice

The computational complexity of the 3D simulation prevents us from any exhaustive analyses for different p and ε_{i}. In order to confirm the results above, a computationally inexpensive 1D periodic lattice in Fig. 11 is considered, whose dispersion equation reads [18],

$$\cos(\beta d_2) = \cos(k_1 d_1)\cos(k_2(d_2 - d_1)) - \frac{\varepsilon_1 + \varepsilon_2}{2\sqrt{\varepsilon_1 \varepsilon_2}} \sin(k_1 d_1)\sin(k_2(d_2 - d_1)), \quad (9)$$

where the wave numbers are $k_1 = k\,(\varepsilon_1)^{1/2}$, $k_2 = k\,(\varepsilon_2)^{1/2}$, the volume fraction of the material with ε_1 and thickness d_1 is $p = d_1/d_2$ and d_2 is the unit cell width. The frequency dependence of the ε_{eff} can therefore be calculated according to $\beta = k\varepsilon_{\text{eff}}^{1/2}$. We can then find out in a similar way the quasi-

Table 1: f_{L}/f_{20} for varying inclusion permittivity ε_{i} and volume fraction p for the 3D composites

p \ ε_{i}	3	10	60
0.1	7	3.5	1.6
0.2	5.2	2.4	1
0.3	4.5	2.1	0.8

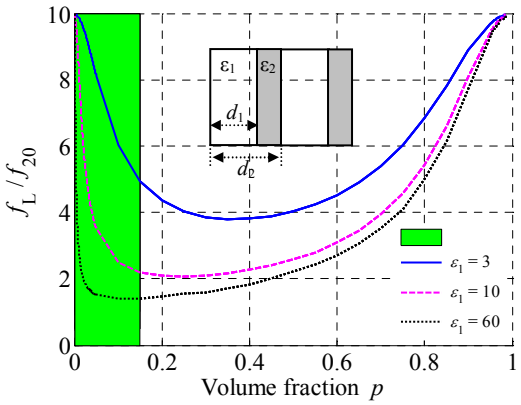

Fig. 11. f_{L}/f_{20} as a function of p and ε_1 for a 1D lattice with $\varepsilon_2 = 1$.

static limit as a function of full sets of p and ε_1. In this case, the satisfactory tolerance is defined as 1% deviation of the quasi-dynamic ε_{eff} from the Maxwell Garnett prediction ($\varepsilon_{\text{MG}} = p\varepsilon_1 + \varepsilon_2 - p\varepsilon_2$), i.e., $|\varepsilon_{\text{eff}} - \varepsilon_{\text{MG}}| \,/\, \varepsilon_{\text{MG}}$. The comparison between Table 1 and Fig. 11 shows that for the same choice of p and ε_{i}, the quasi-static limits f_{L}/f_{20} for the 3D and 1D composites are close to each other despite the obviously geometrical differences. Figure 11, also, supports our remarks in the previous subsection that the increase of the permittivity contrast will reduce the f_{L}/f_{20}, but it does not change monotonously with the volume fraction p for this 1D lattice. The reason we do not observe a similar phenomenon in 3D composites can be explained

as follows. If clusters are not allowed, the maximum p of such composites is about 0.52, with which the ε_i cannot dominate the ε_{eff}. The Rayleigh result, for example at $p = 0.5$, $\varepsilon_e = 1$, and $\varepsilon_i = 60$, is roughly 4.52, which still inclines toward the host permittivity ε_e. Thus, we are in a region similar to the green area in Fig. 11, where f_L/f_{20} decreases monotonously with increasing p.

V. CONCLUSION

The quasi-dynamic approximation of simple composites is studied. By comparing the retrieved quasi-dynamic ε_{eff} with the static Lord Rayleigh prediction, the frequency limit of the quasi-static approximation is then considered.

Moreover, different homogenization methods are developed and validated by a comparison of all the retrieval results. For the slab composite, the conventional NRW method will give rise to FP resonances distorting the result. We present a compensation approach to counteract such an influence, which yields the result matching that by the S_{21} method. The retrieval method involving only S_{21} is a more broadband approach than the others utilizing S_{11}, particularly for these low reflection cases. It also deserves to be mentioned that the retrieval method from only one of the S-parameters may be unstable when the desired permittivity varies over a large dynamical scale, since the algorithm utilized to seek complex roots of Eq. (5) and (6) is sensitive to the initial guess. In particular, at the transparent window when S_{11} equals zero, the ε_{eff} can be separately calculated using the EWR method, which provides a good validation for other retrieval techniques.

For the infinite lattice, the spatial dispersion is smaller than the deviations from the static Rayleigh prediction, shown in Figs. 6 and 8. This phenomenon gives us the possibility of defining a dynamic effective permittivity different from the static one and yet relatively independent of the propagation direction in the quasi-dynamic range.

Finally, the quasi-static approximation limits f_L/f_{20} are calculated for the composites with similar geometry but different permittivity contrasts and inclusion volume fractions, according to the criterion that $|\varepsilon_{eff} - \varepsilon_{Ray}| / \varepsilon_{Ray} \leq 1\%$. Unfortunately, we fail to establish such a definition of the limit that becomes parameter-independent for these composites. It is, however, interesting to find out that when the frequency increases, the stronger the interactions among inclusions are, the quicker the quasi-static approximation will lose its predictive power for the ε_{eff} of the mixtures, if clusters are not allowed. A supplementary 1D lattice is analogically studied to confirm our conclusion. Our parallel work [19] focuses on the influence of finite slab thickness on the homogenization and the characterization of different layers comprising the slab, whose geometry setup is shown in Fig. 1.

ACKNOWLEDGMENT

This work is partially supported by the Academy of Finland.

REFERENCES

[1] G. W. Milton, *The Theory of Composites*, Cambridge University Press, Cambridge, 2002.

[2] A. I. Căbuz, D. Felbacq, and D. Cassagne, "Spatial dispersion in negative-index composite metamaterials," *Phys. Rev. A*, vol. 77, pp. 0138071-01380711, 2008.

[3] J. A. Kong, *Electromagnetic Wave Theory*, EMW Publishing, Cambridge, 2008.

[4] A. Sihvola, *Electromagnetic Mixing Formulas and Applications*, IEE, London, 1999.

[5] J. Zhou, L. Zhang, G. Tuttle, T, Koschny, and C. M. Soukoulis, "Negative index materials using simple short wire pairs," *Phys. Rev. B*, vol. 73, pp. 0411011-0411014, 2006.

[6] T. C. Yang, Y. H. Yang, and T. J. Yen, "An anisotropic negative refractive index medium operated at multiple-angle incidences," *Opt. Express*, vol. 17, pp. 24189-24197, 2009.

[7] D. R. Smith, D. C. Vier, T. Koschny, and C. M. Soukoulis, "Electromagnetic parameter retrieval from inhomogeneous metamaterials," *Phys. Rev, E*, vol. 71, pp. 0366171-03661711, 2005.

[8] C. Menzel, T. Paul, C. Rockstuhl, T. Pertsch, S. Tretyakov, and F. Lederer, "Validity of effective material parameters for optical fishnet metamaterials," *Phys. Rev. B,* vol. 81, pp. 0353201-0353205, 2010.

[9] R. A. Shore and A. D. Yaghjian, "Traveling waves on two- and three- dimensional periodic arrays of lossless scatterers," *Radio Sci.*, vol. 42, pp. RS6S211- RS6S2140, 2007.

[10] Computer Simulation Technology AG, *CST Microwave Studio 2009*, www.cst.com, 2009.

[11] D. Escot, D. Poyatos, I. Montiel, and M. Patricio, "Soft Computing Techniques for Free-Space Measurements of Complex Dielectric Constant," *ACES Journal*, vol. 24, pp. 324-331, 2009.

[12] A. M. Nicolson and G. F. Ross, "Measurement of the intrinsic properties of materials by time-

domain techniques," *IEEE Trans. Inst. Meas.*, vol. 19, pp. 377-382, 1970.

[13] W. B. Weir, "Automatic measurement of complex dielectric constant and permeability at microwave frequencies," *Proceedings of the IEEE*, vol. 62, pp. 33-36, 1974.

[14] D. R. Smith, S. Schultz, P. Markoš, and C. M. Soukoulis, "Determination of effective permittivity and permeability of metamaterials from reflection and transmission coefficients," *Phys. Rev. B*, vol. 65, pp. 1951041-1951045, 2002.

[15] X. Chen, T. M. Grzegorczyk, B.-I. Wu, J. Pacheco, and J. A. Kong, "Robust method to retrieve the constitutive effective parameters of metamaterials," *Phys. Rev. E*, vol. 70, pp. 166081-166087, 2004.

[16] J. D. Joannopoulos, R. D. Meade, and J. N. Winn, *Photonic Crystals*, Princeton University Press, New Jersey, 1995.

[17] C. R. Simovski, "Material parameters of metamaterials," *Opt. and Spectrosc.*, vol. 107, pp. 726-753, 2009.

[18] S. Tretyakov, *Analytical Modeling in Applied Electromagnetics*, Artech House, London, 2003.

[19] H. Kettunen, J. Qi, H. Wallén, and A. Sihvola, "Homogenization of thin dielectric composite slabs: techniques and limitations," Submitted to *ACES Journal*.

Jiaran Qi was born on October 19, 1981, in Harbin, China. He received the B.E. (Communication Engineering) and M.E. degrees (Electromagnetics and Microwave Technology) from Harbin Institute of Technology, China in 2004 and 2006, respectively. He is currently working toward the D.Sc. degree at the Department of Radio Science and Engineering in Aalto University School of Science and Technology (the former Helsinki University of Technology), Finland. His current research interests include electromagnetic wave interaction with complex media, modeling of complex materials, such as composites and metamaterials.

Henrik Kettunen was born in Orimattila, Finland, in 1980. He received the M.Sc. (Tech.) and Lic.Sc. (Tech.) degrees in Electrical Engineering from the Helsinki University of Technology (TKK), Espoo, Finland, in 2006 and 2009, respectively. He is currently working toward the D.Sc. (Tech.) degree in Electrical Engineering at the Aalto University School of Science and Technology, Finland. His research interests include electromagnetic modeling of complex materials.

Henrik Wallén was born in 1975 in Helsinki, Finland. He received the M.Sc. (Tech.) and D.Sc. (Tech.) degrees in Electrical Engineering in 2000 and 2006 from the Helsinki University of Technology (which is now part of Aalto University). He is currently working as a Postdoctoral Researcher at the Aalto University School of Science and Technology, Department of Radio Science and Engineering in Espoo, Finland. He is Secretary of the Finnish National Committee of URSI (International Union of Radio Science). His research interests include electromagnetic theory, modeling of complex materials, and computational electromagnetics.

Ari Sihvola was born on October 6th, 1957, in Valkeala, Finland. He received the degrees of Diploma Engineer in 1981, Licentiate of Technology in 1984, and Doctor of Technology in 1987, all in Electrical Engineering, from the Helsinki University of Technology, Finland.

Besides working for TKK and the Academy of Finland, he was a visiting engineer in the Research Laboratory of Electronics of the Massachusetts Institute of Technology, Cambridge, in 1985–1986, and in 1990–1991, he worked as a visiting scientist at the Pennsylvania State University, State College. In 1996, he was a visiting scientist at the Lund University, Sweden, and in 2000–2001 he was visiting professor at the Electromagnetics and Acoustics Laboratory of the Swiss Federal Institute of Technology, Lausanne. In the summer of 2008, he was visiting professor at the University of Paris XI, France. Ari Sihvola is professor of electromagnetics in Aalto University School of Science and Technology (before 2010 Helsinki University of Technology) with interest

in electromagnetic theory, complex media, materials modeling, remote sensing, and radar applications. He is Chairman of the Finnish National Committee of URSI (International Union of Radio Science) and Fellow of IEEE. He was awarded the five-year Finnish Academy Professor position starting August 2005. Starting January 2008, he is director of the Graduate School of Electronics, Telecommunications, and Automation (GETA).